





Cite this: *Dalton Trans.*, 2018, **47**, 16543

Efficient green photoluminescence and electroluminescence of iridium complexes with high electron mobility†

Hua-Bo Han,^a Zheng-Guang Wu,^a Zhi-Ping Yan,^a Yue Zhao ^a and You-Xuan Zheng ^{*,a,b}

Aiming to balance the injection and transport of electrons and holes, nitrogen heterocycle and 1,3,4-oxadiazole derivatives were introduced in iridium(III) complexes to obtain organic light-emitting diodes (OLEDs) with high performances. Thus, two novel Ir(III) complexes (Ir(tfmppm)₂(pop) and Ir(tfmppm)₂(pop)) with green emissions using 2-(3,5-bis(trifluoromethyl)phenyl)pyrimidine (tfmppm) and 2-(2,6-bis(trifluoromethyl)pyridin-4-yl)pyrimidine (tfmppm) as cyclometalating ligands, and 2-(5-phenyl-1,3,4-oxadiazol-2-yl)phenol (pop) as an ancillary ligand were synthesized. Both emitters show high photoluminescence efficiencies up to 94% and good electron mobility. The devices using two emitters with the structure of ITO (indium-tin-oxide)/MoO₃ (molybdenum oxide, 5 nm)/TAPC (di-[4-(*N,N*-ditolyl-amino)-phenyl]cyclohexane, 30 nm)/mCP (1,3-bis(9*H*-carbazol-9-yl)benzene, 5 nm)/Ir(III) complexes (6 wt%): PPO21 (3-(diphenylphosphoryl)-9-(4-(diphenylphosphoryl)phenyl)-9*H*-carbazole, 10 nm)/TmPyPB (1,3,5-tri(*m*-pyrid-3-yl-phenyl) benzene, 40 nm)/LiF (1 nm)/Al (100 nm) display good electroluminescence performances with a maximum luminance of 48 981 cd m⁻², a maximum current efficiency of 92.79 cd A⁻¹ and a maximum external quantum efficiency up to 31.8%, respectively, and the efficiency roll-off ratio is low, suggesting that they have potential application in OLEDs.

Received 20th July 2018,
Accepted 24th October 2018

DOI: 10.1039/c8dt02961j

rsc.li/dalton

Introduction

Since Tang and VanSlyke fabricated the first high efficiency thin-film organic light-emitting diodes (OLEDs) by the vacuum deposition method in 1987,¹ many types of materials have been extensively investigated because of their great varieties and high emission efficiency. Compared to fluorophores, the phosphorescent transition metal complexes can not only make use of singlet excitons but also harvest triplet excitons to remarkably promote the characteristics of the devices.² Among all these complexes, cyclometalated iridium(III) complexes are

considered as the most fascinating candidates because of their tunable emission energy, excellent chemical stability and high photoluminescence efficiency.³

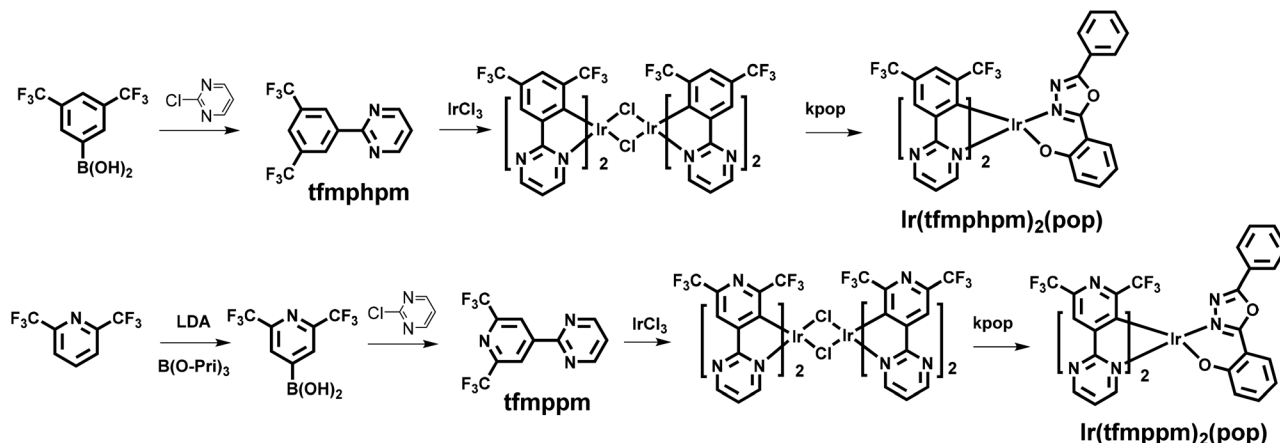
However, the problem of imbalance between the injection and transport of electrons and holes still exists and deeply influences the performances of OLEDs, because the hole mobility of the majority of hole-transporting materials is much higher than the electron mobility of the electron-transporting materials. To avoid a serious efficiency roll-off caused by the charge carrier balance deterioration and nonradioactive quenching processes, the synthesis of dopants with excellent electron mobility is essential to gain efficient phosphorescent OLEDs.⁴

As is well known, the introduction of a nitrogen heterocycle in the ligands would enhance the electron mobility of Ir(III) complexes.⁵ Meanwhile, OLEDs based on Ir(III) complexes with 1,3,4-oxadiazole derivatives as the ancillary ligand always exhibit good performances due to their high electron mobility, high photoluminescence quantum yield and good thermal and chemical stabilities.⁶ Besides that, bulky trifluoromethyl (–CF₃) substituents can affect the molecular packing and the steric protection surrounding the metal would restrain the self-quenching impact, and the C–F bond with a low vibrational frequency can reduce the radiationless deactivation

^aState Key Laboratory of Coordination Chemistry, Jiangsu Key Laboratory of Advanced Organic Materials, Collaborative Innovation Center of Advanced Microstructures, School of Chemistry and Chemical Engineering, Nanjing University, Nanjing 210093, P. R. China. E-mail: yxzhang@nju.edu.cn

^bMaAnShan High-Tech Research Institute of Nanjing University, MaAnShan, 238200, P. R. China

† Electronic supplementary information (ESI) available: The transient EL signals for the device structure of ITO/TAPC (50 nm)/Ir complexes (60 nm)/LiF (1 nm)/Al (100 nm) under different applied fields of Ir(tfmppm)₂(pop) and Ir(tfmppm)₂(pop). The crystallographic data, selected bonds and angles of complexes Ir(tfmppm)₂(pop) and Ir(tfmppm)₂(pop). CCDC 1830696 and 1830699. For ESI and crystallographic data in CIF or other electronic format see DOI: 10.1039/c8dt02961j



Scheme 1 The synthetic routes of ligands and the complexes.

rate.⁷ On this basis, as shown in Scheme 1, two new heteroleptic Ir(III) complexes with 2-(3,5-bis(trifluoromethyl)phenyl)pyrimidine (tfmphpm) and 2-(2,6-bis(trifluoromethyl)pyridin-4-yl)pyrimidine (tfmppm) as cyclometalating ligands and 2-(5-phenyl-1,3,4-oxadiazol-2-yl)phenol (pop) as the ancillary ligand were synthesized and investigated.

Two complexes show green emissions with peaks at 502 and 505 nm with photoluminescence quantum efficiencies of 87% and 94%, respectively. They also have higher electron mobility than the widely used electron transport material of Alq₃ (aluminum 8-hydroxyquinolate). Therefore, for the device G1 based on Ir(tfmphpm)₂(pop), a maximum current efficiency ($\eta_{c,max}$) of 59.82 cd A⁻¹ and a maximum external quantum efficiency (EQE_{max}) of 27.3% were obtained while the device G2 using Ir(tfmppm)₂(pop) as the emitter shows better EL performances with a $\eta_{c,max}$ and an EQE_{max} up to 92.79 cd A⁻¹ and 31.8%, respectively, and the efficiency roll-off is rather low.

Experimental section

Syntheses

All the reagents used were of commercial grade. The ligands and complexes were synthesized under a nitrogen atmosphere and the synthetic routes are listed in Scheme 1. The pop ligand was prepared according to our former publications.⁶

Synthesis of 2-(3,5-bis(trifluoromethyl)phenyl)pyrimidine (tfmphpm). 2-Chloropyrimidine (10 mmol, 1.15 g), bis(diphenylphosphino)ferrocene palladium(II) dichloride (0.3 mmol, 0.22 g) and (3,5-bis(trifluoromethyl)phenyl)boronic acid (12 mmol, 3.10 g) were added into 50 mL THF. After 20 mL of aqueous 2 N K₂CO₃ was added, the reaction mixture was heated at 70 °C for 1 day. The mixture was poured into water and extracted with CH₂Cl₂ (10 mL × 3 times). Finally, silica column purification (PE : EA = 10 : 1) gave 2-(3,5-bis(trifluoromethyl)phenyl)pyrimidine in 89% yield (8.9 mmol, 2.61 g). MS (ESI): calcd for M⁺ (C₁₂H₆F₆N₂)⁺ m/z = 292.18, found 293.17. ¹H NMR (400 MHz, CDCl₃) δ 8.97 (s, 2H), 8.88 (d, J = 4.9 Hz,

2H), 7.99 (s, 1H), 7.32 (t, J = 4.8 Hz, 1H). ¹⁹F NMR (377 MHz, DMSO) δ -61.68 (s). ¹³C NMR (101 MHz, DMSO) δ 160.65 (s), 158.61 (s), 139.94 (s), 131.40 (q, J = 33.1 Hz, 3H), 127.99 (q, J = 3.3 Hz), 124.67 (m), 123.65 (q, J = 273.71 Hz), 121.83 (s).

Synthesis of 2-(2,6-bis(trifluoromethyl)pyridin-4-yl)pyrimidine (tfmppm). A stirred solution of 2,6-bis(trifluoromethyl)pyridine (0.22 g, 10 mmol) in diethyl ether (20 mL) was cooled to -78 °C. LDA (lithium diisopropylamide, 6 mL, 10 mmol) was added over 20 min and stirred for 1 h, and then B(OPr-i)₃ (2.89 mL, 12.4 mmol) was added. The mixture was warmed to room temperature and stirred for another 1 h. The pH was adjusted to 10 by the slow addition of 10% aqueous NaOH solution (20 mL). After 1 hour, the organic phase was acidified to pH = 4 by the dropwise addition of 3 N HCl. The extraction with ethyl acetate and evaporation of the organic phase gave the corresponding crude aryl boronic acids. 2-Chloropyrimidine (10 mmol, 1.15 g), bis(diphenylphosphino)ferrocene palladium(II) dichloride (0.3 mmol, 0.22 g) and boronic acids (12 mmol, 3.52 g) were added into 50 mL THF. After 20 mL of aqueous 2 N K₂CO₃ was added, the reaction mixture was heated at 70 °C for 1 day. The mixture was poured into water and extracted with CH₂Cl₂ (10 mL × 3 times). Finally, silica column purification (PE : EA = 10 : 1) gave 2-(2,6-bis(trifluoromethyl)pyridin-4-yl)pyrimidine in 71% yield (7.1 mmol, 2.10 g). MS (ESI): calcd for M⁺ (C₁₁H₅F₆N₃)⁺ m/z = 293.17, found 294.19. ¹H NMR (400 MHz, CDCl₃) δ 8.94 (d, J = 4.9 Hz, 2H), 8.93 (s, 2H), 7.43 (t, J = 4.9 Hz, 1H). ¹⁹F NMR (377 MHz, DMSO) δ -66.88 (s). ¹³C NMR (101 MHz, DMSO) δ 159.38 (s), 158.92 (s), 149.84 (s), 148.50 (q, J = 35.4 Hz), 123.15 (s), 122.04 (q, J = 2.1 Hz), 121.76 (q, J = 275.73 Hz).

General syntheses of Ir(III) complexes. A mixture of IrCl₃ (1 mmol, 0.30 g) and tfmphpm/tfmppm (2.5 mmol, 0.73 g) in 2-ethoxyethanol and water (20 mL, 3 : 1, v/v) was refluxed for 24 h. After cooling, the solid precipitate was filtered to give the crude cyclometalated Ir(III) chloro-bridged dimer. Then, the slurry of the crude chloro-bridged dimer (0.2 mmol, 0.32 g) and pop potassium salt (0.5 mmol, 0.14 g) in 2-ethoxyethanol (20 mL) was refluxed for 24 h. The solvent was evaporated and

the mixture was poured into water, extracted with CH_2Cl_2 , and then chromatographed to give complexes $\text{Ir}(\text{tfmphpm})_2(\text{pop})$ (0.30 mmol, 0.31 g) and $\text{Ir}(\text{tfmppm})_2(\text{pop})$ (0.28 mmol, 0.29 g), respectively, which were further purified by sublimation under vacuum (4.5×10^5 Pa, 260°C).

$\text{Ir}(\text{tfmphpm})_2(\text{pop})$. 76% yield. ^1H NMR (400 MHz, CDCl_3) δ 8.76 (d, $J = 5.8$ Hz, 1H), 8.72 (dd, $J = 4.7, 2.1$ Hz, 3H), 8.64 (d, $J = 1.6$ Hz, 1H), 7.99–7.95 (m, 1H), 7.74–7.71 (m, 2H), 7.69 (d, $J = 3.7$ Hz, 2H), 7.59 (dd, $J = 8.1, 1.8$ Hz, 1H), 7.53 (ddd, $J = 6.5, 3.8, 1.3$ Hz, 1H), 7.45 (dd, $J = 10.3, 4.6$ Hz, 2H), 7.17 (ddd, $J = 8.7, 6.9, 1.8$ Hz, 1H), 7.03 (dd, $J = 5.8, 4.8$ Hz, 1H), 6.86 (dd, $J = 5.9, 4.7$ Hz, 1H), 6.66 (dd, $J = 8.7, 0.6$ Hz, 1H), 6.52 (ddd, $J = 8.0, 6.9, 1.0$ Hz, 1H). ^{13}C NMR (101 MHz, CDCl_3) δ 175.24, 174.59, 167.06, 163.29, 159.29, 157.98, 157.61, 156.93, 156.43, 148.97, 135.91, 134.57, 132.63, 129.23, 127.12, 126.78, 125.15, 122.62, 122.13, 117.78, 117.26, 115.25, 106.20. ^{19}F NMR (377 MHz, DMSO) δ –58.16 (s), –58.90 (s), –60.94 (s), –61.13 (s). MS (ESI) m/z calcd for $\text{C}_{38}\text{H}_{19}\text{F}_{12}\text{IrN}_6\text{O}_2$: 1011.81 $[\text{M}]^+$, found 1012.93 $[\text{M} + \text{H}]^+$. Anal. calcd For $\text{C}_{38}\text{H}_{19}\text{F}_{12}\text{IrN}_6\text{O}_2$: C 45.11, H 1.89, N 8.31. Found: C 45.08, H 2.16, N 8.39.

$\text{Ir}(\text{tfmppm})_2(\text{pop})$. 71% yield. ^1H NMR (400 MHz, CDCl_3) δ 8.88–8.79 (m, 3H), 8.60 (s, 1H), 8.52 (s, 1H), 8.13–8.05 (m, 1H), 7.76–7.69 (m, 2H), 7.61 (dd, $J = 8.1, 1.7$ Hz, 1H), 7.59–7.52 (m, 1H), 7.47 (t, $J = 7.5$ Hz, 2H), 7.21 (qd, $J = 3.4, 1.9$ Hz, 2H), 7.05 (dd, $J = 5.9, 4.8$ Hz, 1H), 6.67 (d, $J = 8.2$ Hz, 1H), 6.61–6.51 (m, 1H). ^{13}C NMR (101 MHz, acetone) δ 174.97, 174.25, 168.08, 165.42, 161.05, 160.62, 160.22, 159.03, 153.47, 146.87, 142.01, 136.23, 134.36, 131.04, 129.56, 128.38, 125.88, 125.36, 124.37, 122.57, 122.01, 120.40, 119.73, 117.29, 108.55. ^{19}F NMR (377 MHz, DMSO) δ –62.74 (s), –63.42 (s), –66.20 (s), –66.37 (s). MS (ESI) m/z calcd for $\text{C}_{36}\text{H}_{17}\text{F}_{12}\text{IrN}_8\text{O}_2$: 1013.78 $[\text{M}]^+$, found 1014.89 $[\text{M} + \text{H}]^+$. Anal. calcd For $\text{C}_{36}\text{H}_{17}\text{F}_{12}\text{IrN}_8\text{O}_2$: C 42.65, H 1.69, N 11.05. Found: C 42.49, H 1.99, N 11.34.

Results and discussion

Preparation and characterization of compounds

Scheme 1 shows the synthetic route to ligands, $\text{Ir}(\text{tfmphpm})_2(\text{pop})$ and $\text{Ir}(\text{tfmppm})_2(\text{pop})$ complexes. Both the new compounds were further purified by vacuum sublimation and fully characterized by ^1H NMR spectrometry, and the crystal structures further confirmed the identity of the complexes.

Single crystals of $\text{Ir}(\text{tfmphpm})_2(\text{pop})$ and $\text{Ir}(\text{tfmppm})_2(\text{pop})$ were obtained by vacuum sublimation and the crystal diagrams are displayed in Fig. 1. The molecular parameters and atomic coordinates are shown in Table S1.† From the structure diagrams of crystals it can be found that the iridium atom is embraced by C, N and O atoms from $\text{tfmphpm}/\text{tfmppm}$ and pop , with a twisted octahedral coordination geometry. For $\text{Ir}(\text{tfmphpm})_2(\text{pop})$ and $\text{Ir}(\text{tfmppm})_2(\text{pop})$, the angles of $[\text{N}–\text{Ir}–\text{O}]$ are $85.8(2)^\circ$ – $86.78(12)^\circ$, and the angles of $[\text{C}–\text{Ir}–\text{N}]$ are $80.2(2)^\circ$ – $81.38(14)^\circ$. The lengths of Ir–C bonds range from 2.034(4) to 2.064(4) Å. The Ir–N bonds have the lengths of 2.026(4)–2.107(3) Å. The lengths of Ir–O bonds are 2.105 Å–

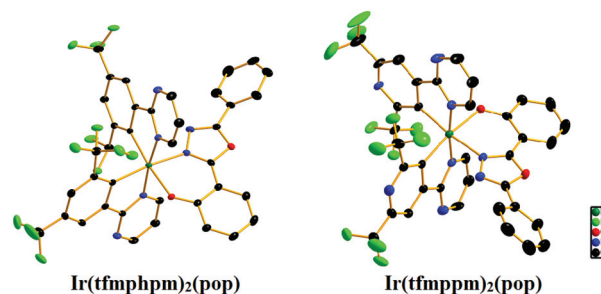


Fig. 1 Oak Ridge Thermal Ellipsoidal Plot (ORTEP) diagram of $\text{Ir}(\text{tfmphpm})_2(\text{pop})$ (CCDC No. 1830696†) and $\text{Ir}(\text{tfmppm})_2(\text{pop})$ (CCDC No. 1830699†). Hydrogen atoms are omitted for clarity. Ellipsoids are drawn at the 30% probability level.

2.117(3) Å. These results are similar to the parameters of the cyclometalated $\text{Ir}(\text{III})$ complexes that have been reported.

Thermal stability

Good thermal stability of the materials is a necessary prerequisite for efficient and stable OLEDs. If a complex can be applied in practical OLEDs, the decomposition temperature (T_d) needs to be high enough to guarantee that the complex could be deposited onto the solid face without any decomposition on sublimation. The thermogravimetric analysis (TGA) curves of $\text{Ir}(\text{tfmphpm})_2(\text{pop})$ and $\text{Ir}(\text{tfmppm})_2(\text{pop})$ are shown in Fig. 2. It can be figured out that there is no loss observed below 290°C in weight from the curves of TGA for $\text{Ir}(\text{tfmphpm})_2(\text{pop})$ and the decomposition temperature (5% loss of weight) is 312°C for $\text{Ir}(\text{tfmphpm})_2(\text{pop})$. However, there is no loss in weight observed below 320°C from the curves of TGA for $\text{Ir}(\text{tfmppm})_2(\text{pop})$, and the decomposition temperature (5% loss of weight) improves to 354°C for $\text{Ir}(\text{tfmppm})_2(\text{pop})$. The good thermal stability suggests that both complexes have potential application in OLEDs.

Electrochemical properties and theoretical calculation

The highest occupied molecular orbital (HOMO) and lowest unoccupied molecular orbital (LUMO) energy levels of the dopants will guide in designing the structure of the OLED. Cyclic voltammetry was used to test the oxidation peak poten-

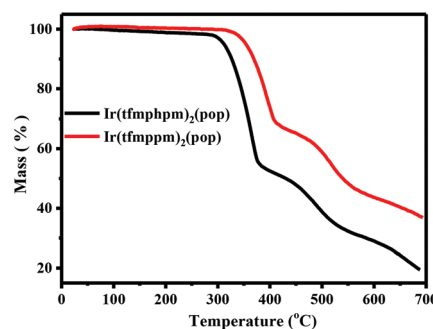


Fig. 2 The TGA curves of $\text{Ir}(\text{tfmphpm})_2(\text{pop})$ and $\text{Ir}(\text{tfmppm})_2(\text{pop})$ (the heating rate is 20°C per minute).

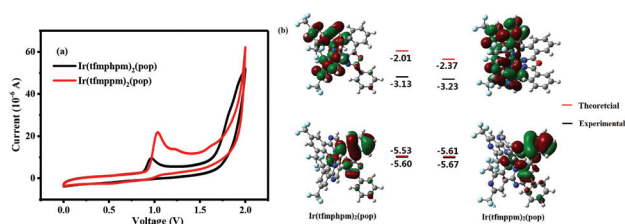


Fig. 3 (a) The cyclic voltammogram curves and (b) contour plots of Ir(tfmphpm)₂(pop) and Ir(tfmppm)₂(pop).

tial (E_{ox}) of Ir(tfmphpm)₂(pop) and Ir(tfmppm)₂(pop). The HOMO levels were calculated from the E_{ox} and the band gaps (E_g), which were estimated from the UV-vis absorption edges.⁸ Then the LUMO levels were determined according to the equation $\text{LUMO} = \text{HOMO} + E_g$. The oxidation potentials of Ir(tfmphpm)₂(pop) and Ir(tfmppm)₂(pop) (Fig. 3(a)) were found to be 0.97 V and 1.12 V, respectively, which can be ascribed to the metal-centered Ir(III)/Ir(IV) oxide couple, consistent with the cyclometalated Ir(III) system reported.⁹ However, the reduction peaks of Ir(tfmphpm)₂(pop) and Ir(tfmppm)₂(pop) are not obvious, demonstrating that the redox process is not completely reversible, which is also observed in related Ir(III) complexes containing oxadiazole units.¹⁰ The HOMO/LUMO energy levels are calculated as -5.60/-3.13 eV and -5.67/-3.23 eV, respectively, for Ir(tfmphpm)₂(pop) and Ir(tfmppm)₂(pop). With a lower LUMO level which can benefit the trapping of electrons and broaden the recombination zone, the device based on Ir(tfmppm)₂(pop) would show better performances. What's more, the difference between the E_g of the complexes, which contributes to the variations of the PL spectra, is small. Thus, the introduction of the special one more nitrogen atom has almost no effect on the emission spectra for the two complexes.

To provide deep understanding about the nature of the excited states of these complexes, the density functional theory (DFT) calculations¹¹ for both were conducted employing the Gaussian09 software with the B3LYP functional.¹² Plots of the HOMO/LUMO and the molecular orbital energy levels are presented in Fig. 3(b). The basis set used for C, H, N, O and F atoms was 6-31G(d, p) while the LanL2DZ basis set was employed for iridium atoms.¹³ The solvent effect of CH₂Cl₂ was taken into consideration using a conductor like polarizable continuum model (C-PCM). It can be observed from the theoretical calculation that nearly all LUMOs are on the cyclometalating ligands (90.57/94.84%) and HOMOs are mostly situated on the ancillary ligand (80.62/81.78%). The rising compositions of HOMOs on the ancillary ligand make the electrochemical oxidation processes occur on both metal centered orbitals and the ancillary ligand, leading to the irreversible redox processes of the Ir(III) complexes.

Photophysical properties

The UV-vis absorption and photoluminescence spectra of two complexes Ir(tfmphpm)₂(pop) and Ir(tfmppm)₂(pop) in CH₂Cl₂ (5×10^{-5} M) at room temperature are shown in Fig. 4.

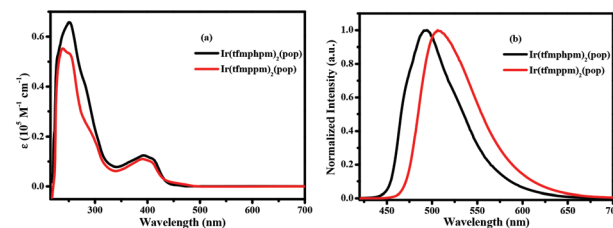


Fig. 4 (a) The UV-vis absorption and (b) emission spectra of Ir(tfmphpm)₂(pop) and Ir(tfmppm)₂(pop) complexes in degassed CH₂Cl₂ solutions (5.0×10^{-5} mol L⁻¹) at room temperature.

The absorption spectra of the two complexes show broad and intense bands below 340 nm, assigned to the spin-allowed intraligand ¹LC ($\pi \rightarrow \pi^*$) transitions of tfmphpm/tfmppm and pop ligands. The weak bands lasting to 520 nm can be assigned to spin-allowed metal-ligand charge transfer (¹MLCT) and spin forbidden ³MLCT transition bands caused by the large spin orbital coupling (SOC) that was introduced by the Ir(III) center.¹⁴ The strongest emission peaks at 494 nm and 506 nm in CH₂Cl₂, respectively, were produced by the electronic transition between the lowest triplet excited state and the ground state, which make Ir(tfmphpm)₂(pop) and Ir(tfmppm)₂(pop) green phosphors. From Fig. S1 (ESI†) and Table 1, it can be seen that the PL spectra of Ir(tfmphpm)₂(pop) and Ir(tfmppm)₂(pop) at 77 K become structured compared with those at room temperature. In general, the emission bands from the MLCT states are broad and featureless, whereas a highly structured emission band mainly originates from the ³ $\pi-\pi^*$ state. Accordingly, the complexes Ir(tfmphpm)₂(pop) and Ir(tfmppm)₂(pop) emit from a mixture of MLCT states and the ligand-based ³ $\pi-\pi^*$ state. This indicates that the MLCT characters involved in the emitting T₁ states of different complexes are various but significant, since a dominant MLCT character in T₁ usually leads to large inhomogeneity and low-energy lying metal-ligand vibrational satellites, smearing out the spectrum below the electronic original emission. Although the structures are different, the emissions of Ir(tfmphpm)₂(pop) and Ir(tfmppm)₂(pop) are analogous, which are consistent with their electrochemical results.

Both complexes show high quantum efficiencies up to 0.87 and 0.94 for Ir(tfmphpm)₂(pop) and Ir(tfmppm)₂(pop), respectively, suggesting that they are potential emitters for efficient devices. Furthermore, the phosphorescence lifetime (τ) is the crucial factor that determines the rate of triplet-triplet annihilation in OLEDs. Longer τ values usually cause greater triplet-triplet annihilation. The lifetimes of the complexes Ir(tfmphpm)₂(pop) and Ir(tfmppm)₂(pop) are in the range of microseconds (1.00 and 0.93 μ s in CH₂Cl₂ solution, respectively) at room temperature (Fig. S2† and Table 1) and are indicative of the phosphorescence origin for the excited states in each case.

Electron mobility

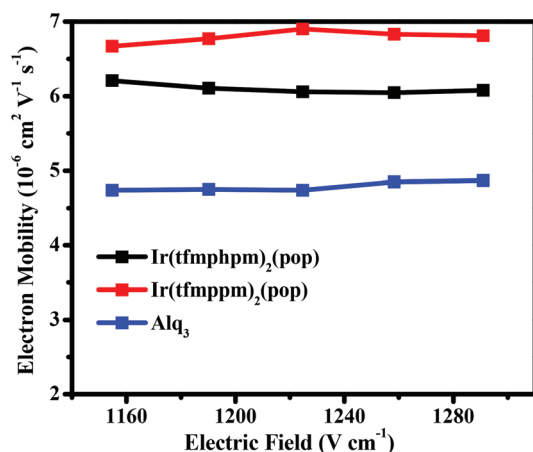
An excellent electron mobility of the emitter could benefit electron transport, which would balance the injection and trans-

Table 1 Photophysical data of Ir(III) complexes

Complex	T_d^a (°C)	λ_{abs}^b (nm)	λ_{em}^c (nm)		Φ^d (%)	τ^e (μs)	HOMO/LUMO ^f (eV)
			298 K	77 K			
Ir(tfmphpm) ₂ (pop)	312	250/393	494	486/507/521	87	1.00	−5.60/−3.13
Ir(tfmppm) ₂ (pop)	354	238/391	506	512	94	0.93	−5.67/−3.23

^a T_d : decomposition temperature. ^b Measured in degassed CH₂Cl₂ solution at a concentration of 5×10^{-5} mol L^{−1} at room temperature. ^c Measured in degassed CH₂Cl₂ solution at a concentration of 5×10^{-5} mol L^{−1} at 298 K and 77 K, respectively. ^d Emission quantum yields were measured relative to Ir(ppy)₃ ($\Phi = 0.4$) in degassed CH₂Cl₂ solution at room temperature. ^e Measured in degassed CH₂Cl₂ solution at a concentration of 5×10^{-5} mol L^{−1} at room temperature. ^f From the onset of oxidation potentials of the cyclovoltammetry (CV) diagram using ferrocene as the internal standard and the optical band gap from the absorption spectra in degassed CH₃CN solution.

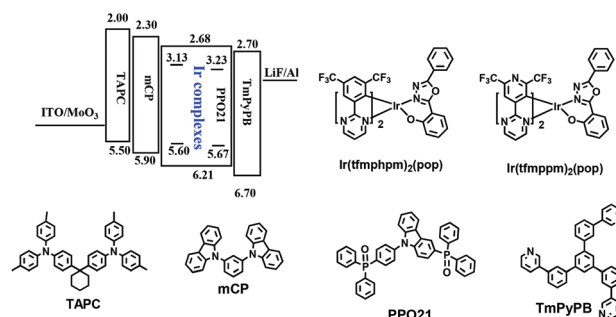
port of electrons and holes, in favour of the enhancement of the device efficiency.¹⁵ To determine their electron mobility values, the transient electroluminescence (TEL) measurement was carried out *via* the devices with a structure of ITO (indium–tin–oxide)/TAPC (1,1-bis[4-*N,N*-di(*p*-tolyl)amino]pyridin-4-yl] cyclohexane, 50 nm)/Ir(III) complexes (60 nm)/LiF (1 nm)/Al (100 nm).¹⁶ The Ir(III) complexes act as not only the emissive layers (EML) but also electron-transport layers. The experimental results (Fig. 5) indicated that the electron mobility values of Ir(tfmphpm)₂(pop) and Ir(tfmppm)₂(pop) are $6.05\text{--}6.21 \times 10^{-6}$ cm² V^{−1} s^{−1} and $6.67\text{--}6.90 \times 10^{-6}$ cm² V^{−1} s^{−1}, respectively, under the electric field from 1040 (V cm^{−1})^{1/2} to 1300 (V cm^{−1})^{1/2}, higher than that of the electron transport material Alq₃ (aluminum 8-hydroxyquinolate, $4.74\text{--}4.87 \times 10^{-6}$ cm² V^{−1} s^{−1}).¹⁷ Additionally, the electron mobility of Ir(tfmppm)₂(pop) is higher than that of Ir(tfmphpm)₂(pop) by introducing one more nitrogen heterocycle to the cyclometalating ligand. These results exactly fit our design intended to improve the electron transport ability of the emitter. The good electron transport ability of Ir(tfmphpm)₂(pop) and Ir(tfmppm)₂(pop) will reinforce the recombination chance of electrons and holes, so that their devices may show good performances, especially for the device based on Ir(tfmppm)₂(pop).

**Fig. 5** Electric field dependence of charge electron mobility in the thin films of Ir(tfmphpm)₂(pop), Ir(tfmppm)₂(pop) and Alq₃.

OLED performance

To evaluate the EL performances of the two complexes, single emitting layer (EML) devices named G1 and G2 using Ir(tfmphpm)₂(pop) and Ir(tfmppm)₂(pop) as the emitters, respectively, were fabricated with the structure of ITO/MoO₃ (molybdenum oxide, 5 nm)/TAPC (30 nm)/Ir complexes (*x* wt%):PPO21 (10 nm)/TmPyPB (40 nm)/LiF (1 nm)/Al (100 nm). MoO₃ and LiF served as hole- and electron-injection interface modified materials, respectively. TAPC possessing high hole mobility (1×10^{-2} cm² V^{−1} s^{−1}) and a high-lying LUMO level (−2.0 eV) was used as the hole transport/electron block layer (HTL/EBL), while TmPyPB with high electron mobility (1×10^{-3} cm² V^{−1} s^{−1}) and a low-lying HOMO level (−6.7 eV) was used as an electron transport/hole block layer (ETL/HBL). The chemical structures of the materials mentioned above as well as the device structure and energy level diagrams are depicted in Fig. 6.

Theoretically speaking, the stepwise HOMO levels of TAPC (−5.50 eV), mCP (−5.90 eV) and PPO21 (−6.21 eV) are beneficial for the injection and transport of holes, while the stepwise LUMO levels of TmPyPB (−2.70 eV) and PPO21 (−2.68 eV) are beneficial for the injection and transport of electrons. Therefore, balanced distribution of carriers (holes and electrons) and a wide recombination zone could be expected. More importantly, the LUMO level of TAPC is 0.3 eV higher than that of mCP which was added to lower the HOMO energy barrier between TAPC and PPO21. The HOMO level of TmPyPB

**Fig. 6** Energy level diagram of HOMO and LUMO levels (relative to the vacuum level) for materials investigated in this work and their molecular structures.

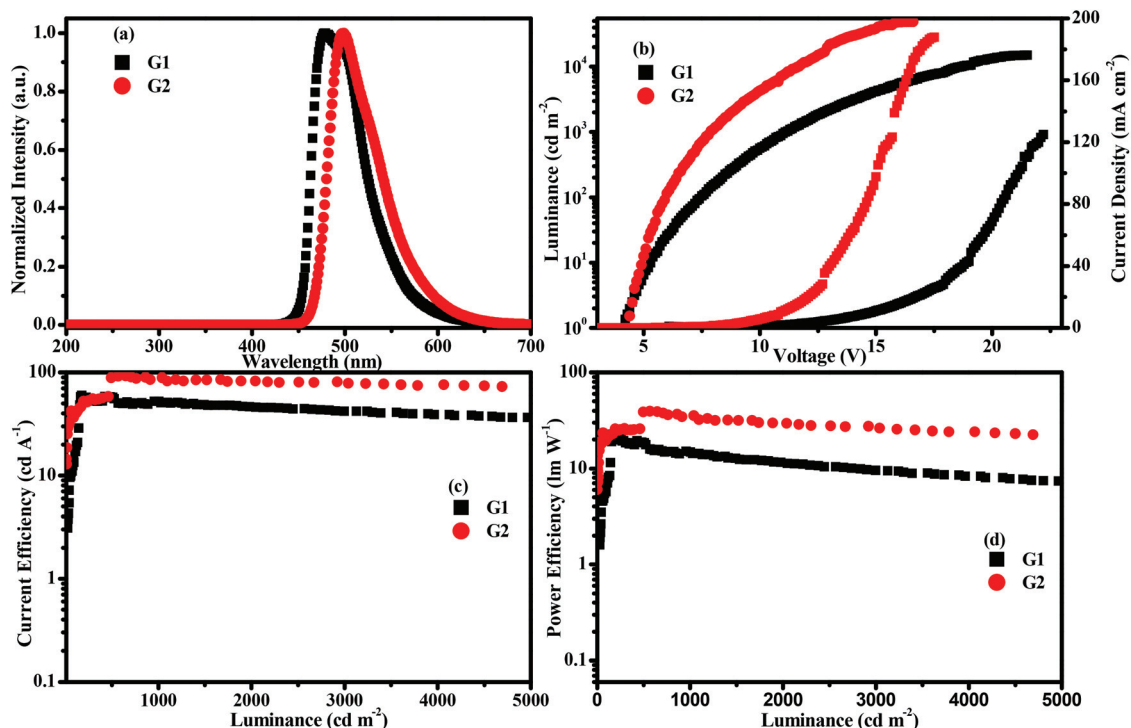


Fig. 7 Characteristics of devices G1 and G2: (a) electroluminescence spectra at 8 V; (b) luminance–voltage–current density (L – V – J) curves; (c) current efficiency–luminance (η_c – L) curves; and (d) power efficiency–luminance (η_p – L) curves.

is 0.49 eV lower than that of PPO21. Thus, holes and electrons are well confined within EMLs and the triplet exciton quenching of the dopants will be effectively avoided. In the devices, the optimized Ir(III) complex doping concentrations are 6 wt% for both complexes Ir(tfmppm)₂(pop) and Ir(tfmppm)₂(pop).

The EL spectra, luminance–voltage–current density (L – V – J) curves, current efficiency–luminance (η_c – L) curves, and power efficiency–luminance (η_p – L) curves for G1 and G2 are shown in Fig. 7, and the crucial EL data are shown in Table 2. The peaks of EL emission are 478 nm and 499 nm for G1 and G2, respectively, which are almost invariant of the current density and there is no dependence on doped concentrations. From Fig. 7(a), it can be seen that the EL spectra are almost identical to the PL spectra of the complexes, suggesting that the EL emissions of the devices arise from the triplet excited states of the phosphors. The Commission Internationale de l'Eclairage (CIE) color coordinates of G1 and G2 are (0.152 and 0.384) and (0.210 and 0.560), respectively.

From Fig. 7 and Table 2, it can be found that the devices based on both complexes with pop as an ancillary ligand show good performances with low roll-off. For device G1, a maximum current efficiency ($\eta_{c,max}$) of 59.82 cd A^{−1}, a maximum external quantum efficiency (EQE_{max}) of 27.3%, a maximum power efficiency ($\eta_{p,max}$) of 22.91 lm W^{−1} and a maximum luminance (L_{max}) of 15 003 cd m^{−2} were obtained, while device G2 using Ir(tfmppm)₂(pop) as the emitter shows better EL performances with a L_{max} , a $\eta_{c,max}$, a $\eta_{p,max}$ and an EQE_{max} up to 48 981 cd m^{−2}, 92.79 cd A^{−1}, 39.46 lm W^{−1} and 31.8%, respectively. Moreover, G2 can retain its high efficiency even at relatively high luminance and the EL efficiency roll-off is rather low. For instance, the current efficiencies for the device G2 still remain as high as 89.20 cd A^{−1} at the brightness of 1000 cd m^{−2} and 63.53 cd A^{−1} at the brightness of 10 000 cd m^{−2}, respectively.

Considering the difference between the structures of both emitters, the introduction of one more nitrogen heterocycle to the cyclometalating ligand does affect the nature of Ir

Table 2 EL performances of devices G1 and G2

Device	$V_{turn-on}^a$ (V)	L_{max}^b (cd m ^{−2})	$\eta_{c,max}^c$ (cd A ^{−1}) (EQE _{max} ^d)	$\eta_{c,L1000}^e$ (cd A ^{−1}) (EQE _{L1000} ^f)	$\eta_{p,max}^g$ (lm W ^{−1})	CIE ^h (x,y)
G1	4.1	15 003	59.82 (27.3%)	52.56 (24.0%)	22.91	0.152, 0.384
G2	4.3	48 981	92.79 (31.8%)	89.20 (30.5%)	39.46	0.210, 0.560

^a Turn-on voltage recorded at a luminance of 1 cd m^{−2}. ^b Maximum luminance. ^c Maximum current efficiency. ^d Maximum external quantum efficiency (EQE_{max}). ^e Current efficiency at 1000 cd m^{−2}. ^f EQE at 1000 cd m^{−2}. ^g Maximum power efficiency. ^h Commission Internationale de l'Eclairage coordinates (CIE).

(tfmppm)₂(pop), which can not only enhance the PL quantum efficiency, but also increase the electron mobility of the Ir(III) complexes, resulting in excellent EL performances. The better electron mobility and the lower LUMO level of Ir(tfmppm)₂(pop) would facilitate the injection and transport of electrons, which would broaden the recombination zone and balance the distribution of holes and electrons, particularly at a high doping concentration, leading to the suppressed triplet-triplet annihilation (TTA) and triplet-polaron annihilation (TPA) effects, resulting in excellent EL performances, consistent with the design intention.

Conclusions

In conclusion, two bis-cyclometalated Ir(III) complexes Ir(tfmppm)₂(pop) and Ir(tfmppm)₂(pop) with 2-(3,5-bis(trifluoromethyl)phenyl)pyrimidine (tfmppm) and 2-(2,6-bis(trifluoromethyl)pyridin-4-yl)pyrimidine (tfmppm) as cyclometalating ligands and 2-(5-phenyl-1,3,4-oxadiazol-2-yl)phenol (pop) as the ancillary ligand were reported. Both complexes emit green phosphorescence with high quantum efficiencies up to 94%. By introducing one more nitrogen heterocycle to the cyclometalating ligand, Ir(tfmppm)₂(pop) attains better electron mobility and a lower LUMO level, which would facilitate the injection and transport of electrons to broaden the recombination zone and balance the distribution of holes and electrons. As a result, device G2 based on Ir(tfmppm)₂(pop) as the emitter shows better EL performances with the maximum luminance, current efficiency, power efficiency and external quantum efficiency up to 48 981 cd m⁻², 92.79 cd A⁻¹, 39.46 lm W⁻¹ and 31.8%, respectively. Moreover, the η_c and EQE of the device G2 can still be retained as high as 89.20 cd A⁻¹ and 30.5%, respectively, at the practical luminance of 1000 cd m⁻².

Conflicts of interest

There are no conflicts to declare.

Acknowledgements

This work was supported by the National Natural Science Foundation of China (51773088), the Natural Science Foundation of Jiangsu Province (BY2016075-02) and the Fundamental Research Funds for the Central Universities (020514380131).

Notes and references

- 1 C. W. Tang and S. A. VanSlyke, *Appl. Phys. Lett.*, 1987, **51**, 913.
- 2 (a) Y. Sun, N. C. Giebink, H. Kanno, B. Ma, M. E. Thompson and S. R. Forrest, *Nature*, 2006, **440**, 908; (b) V. N. Kozhevnikov, Y. H. Zheng and A. P. Monkman, *Chem. Mater.*, 2013, **25**, 2352; (c) B. H. Zhan, G. P. Tan, C. S. Lam, B. Yao, C. L. Ho, L. H. Liu, Z. Y. Xie, W. Y. Wong, J. Q. Ding and L. Wang, *Adv. Mater.*, 2012, **24**, 1873; (d) S. Reineke, F. Lindner, G. Schwartz, N. Seidler, K. Walzer, B. Luessem and K. Leo, *Nature*, 2009, **459**, 234; (e) G. Schwartz, S. Reineke and T. C. Rosenow, *Adv. Funct. Mater.*, 2009, **19**, 1319; (f) M. A. Baldo, D. F. O'Brien, Y. You, A. Shoustikov, S. Sibley, M. E. Thompson and S. R. Forrest, *Nature*, 1998, **395**, 151; (g) Y. Ma, H. Zhang, J. Shen and C. Che, *Synth. Met.*, 1998, **94**, 245; (h) C. Adachi, M. A. Baldo, M. E. Thompson and S. R. Forrest, *J. Appl. Phys.*, 2001, **90**, 5048.
- 3 (a) S. Lamansky, P. Djurovich, D. Murphy, F. Abdel-Razzaq, H. E. Lee, C. Adachi, P. E. Burrows, S. R. Forrest and M. E. Thompson, *J. Am. Chem. Soc.*, 2001, **123**, 4304; (b) J. Li, P. I. Djurovich, B. D. Alleyne, M. Yousufuddin, N. N. Ho, J. C. Thomas, J. C. Peters, R. Bau and M. E. Thompson, *Inorg. Chem.*, 2005, **44**, 1713; (c) D. B. Xia, B. Wang, B. Chen, S. M. Wang, B. H. Zhang, J. Q. Ding, L. X. Wang, X. B. Jing and F. S. Wang, *Angew. Chem., Int. Ed.*, 2014, **53**, 1048; (d) X. B. Xu, G. J. Zhou and W. Y. Wong, *Chem. Commun.*, 2014, **50**, 2473; (e) R. J. Wang, D. Liu and J. Y. Li, *Adv. Mater.*, 2011, **23**, 2823; (f) S. Haneder, E. D. Como and J. Feldmann, *Adv. Mater.*, 2008, **20**, 3325; (g) J. Q. Ding, B. Wang and L. X. Wang, *Angew. Chem., Int. Ed.*, 2009, **48**, 6664; (h) W. Y. Wong, C. L. Ho and Z. Y. Lin, *Angew. Chem., Int. Ed.*, 2006, **45**, 7800; (i) W. W. Tian, W. Jiang and Y. M. Sun, *J. Mater. Chem. C*, 2014, **2**, 1104; (j) J. J. Kim, Y. You, Y. S. Park, J. J. Kim and S. Y. Park, *J. Mater. Chem.*, 2009, **19**, 8347; (k) Z. Q. Chen, Z. Q. Bian and C. H. Huang, *Adv. Mater.*, 2010, **22**, 1534; (l) S. M. Chen, G. P. Tan, W. Y. Wong and H. S. Kwok, *Adv. Funct. Mater.*, 2011, **21**, 3785; (m) J. M. Fernández-Hernández, C. H. Yang, J. I. Beltrán, V. Lemaure, F. Polo, R. Fröhlich, J. Cornil and L. D. Cola, *J. Am. Chem. Soc.*, 2011, **133**, 10543; (n) K. Y. Lu, H. H. Chou, C. H. Hsieh, Y. H. O. Yang, H. R. Tsai, H. Y. Tsai, L. C. Hsu, C. Y. Chen, I. C. Chen and C. H. Cheng, *Adv. Mater.*, 2011, **23**, 4933; (o) S. Lee, S. O. Kim, H. Shin, H. J. Yun, K. Yang, S. K. Kwon, J. J. Kim and Y. H. Kim, *J. Am. Chem. Soc.*, 2013, **135**, 14321; (p) X. L. Yang, N. Sun, J. S. Dang, Z. Huang, C. L. Yao, X. B. Xu, C. L. Ho, G. J. Zhou, D. G. Ma, X. Zhao and W. Y. Wong, *J. Mater. Chem. C*, 2013, **1**, 3317; (q) H. Sasabe, H. Nakanishi, Y. Watanabe, S. Yano, M. Hirasawa, Y. J. Pu and J. Kido, *Adv. Funct. Mater.*, 2013, **23**, 5550; (r) H.-H. Chou, Y.-K. Li, Y.-H. Chen, C.-C. Chang, C.-Y. Liao and C.-H. Cheng, *ACS Appl. Mater. Interfaces*, 2013, **5**, 6168; (s) V. K. Rai, M. Nishiura, M. Takimoto and Z. Hou, *J. Mater. Chem. C*, 2014, **2**, 5317; (t) H. Cao, H. Sun, Y. Yin, X. Wen, G. Shan, Z. Su, R. n. Zhong, W. Xie, P. Li and D. Zhu, *J. Mater. Chem. C*, 2014, **2**, 2150; (u) A. Graf, P. Liehm, C. Murawski, S. Hofmann, K. Leo and M. C. Gather, *J. Mater. Chem. C*, 2014, **2**, 10298; (v) X. Yang, G. Zhou and W.-Y. Wong, *J. Mater. Chem. C*, 2014, **2**, 1760; (w) P.-N. Lai, C. H. Brysacz, M. K. Alam, N. A. Ayoub, T. G. Gray, J. Bao and T. S. Teets, *J. Am. Chem. Soc.*, 2018,

- 140, 10198; (x) H. Na and T. S. Teets, *J. Am. Chem. Soc.*, 2018, **140**, 6353.
- 4 (a) S. Heun and P. M. Borsenberger, *Chem. Phys.*, 1995, **200**, 245; (b) H. H. Fong, K. C. Lun and S. K. So, *Chem. Phys. Lett.*, 2002, **353**, 407.
- 5 (a) Y. Yamashita, *Chem. Lett.*, 2009, **38**, 870; (b) A. V. Lonchakov, O. A. Rakitin, N. P. Gritsan and A. V. Zibarev, *Molecules*, 2013, **18**, 9850; (c) R. Benassi, P. Ferrarini, C. Fontanesi, L. Benedetti and F. Paolucci, *J. Electroanal. Chem.*, 2004, **564**, 231; (d) T. L. Kunii and H. Kuroda, *Theor. Chim. Acta*, 1968, **11**, 106.
- 6 (a) Y.-M. Jing, C.-C. Wang, L.-S. Xue, T.-Y. Li, S. Zhang, X. Liu, X. Liang, Y.-X. Zheng and J.-L. Zuo, *J. Organomet. Chem.*, 2014, **765**, 39; (b) Z. He, W. Y. Wong, X. Yu, H. S. Kwok and Z. Lin, *Inorg. Chem.*, 2006, **45**, 10922; (c) W. Y. Wong, Z. He, S. K. So, K. L. Tong and Z. Lin, *Organometallics*, 2005, **24**, 4079; (d) H.-Y. Li, T.-Y. Li, M.-Y. Teng, Q.-L. Xu, S. Zhang, Y.-M. Jin, X. Liu, Y.-X. Zheng and J.-L. Zuo, *J. Mater. Chem. C*, 2014, **2**, 1116; (e) X. Liu, S. Zhang, Y.-M. Jin, G.-Z. Lu, L. Jiang, X. Liang, Q.-L. Xu and Y.-X. Zheng, *J. Organomet. Chem.*, 2015, **785**, 11.
- 7 Y. T. Tao, C. L. Yang and J. G. Qin, *Chem. Soc. Rev.*, 2011, **40**, 2943–2970.
- 8 P. Brulatti, R. J. Gildea, J. A. K. Howard, V. Fattori, M. Cocchi and J. A. Gareth Williams, *Inorg. Chem.*, 2012, **51**, 3813.
- 9 S. Bettington, M. Tavasli, M. R. Bryce, A. Beeby, H. Al-Attar and A. P. Monkman, *Chem. – Eur. J.*, 2007, **13**, 1423.
- 10 (a) L. Q. Chen, H. You, C. L. Yang, D. G. Ma and J. G. Qin, *Chem. Commun.*, 2007, 1352; (b) L. Q. Chen, C. L. Yang, M. Li, J. G. Qin, J. Gao, H. You and D. G. Ma, *Cryst. Growth Des.*, 2007, **7**, 39; (c) Z. Xu, Y. Li, X. Ma, X. Gao and H. Tian, *Tetrahedron*, 2008, **64**, 1860; (d) Y. H. Zheng, A. S. Batsanov and M. R. Bryce, *Inorg. Chem.*, 2011, **50**, 3354; (e) Q. L. Xu, H. Y. Li, C. C. Wang, S. Zhang, T. Y. Li, Y. M. Jing, Y. X. Zheng, W. Huang, J. L. Zuo and X. Z. You, *Inorg. Chim. Acta*, 2012, **391**, 50.
- 11 E. Runge and E. K. U. Gross, *Phys. Rev. Lett.*, 1984, **52**, 997.
- 12 M. J. Frisch, G. W. Trucks, H. B. Schlegel, G. E. Scuseria, M. A. Robb, J. R. Cheeseman, G. Scalmani, V. Barone, B. Mennucci, G. A. Petersson, H. Nakatsuji, M. Caricato, X. Li, H. P. Hratchian, A. F. Izmaylov, J. Bloino, G. Zheng, J. L. Sonnenberg, M. Hada, M. Ehara, K. Toyota, R. Fukuda, J. Hasegawa, M. Ishida, T. Nakajima, Y. Honda, O. Kitao, H. Nakai, T. Vreven, J. A. Montgomery Jr., J. E. Peralta, F. Ogliaro, M. Bearpark, J. J. Heyd, E. Brothers, K. N. Kudin, V. N. Staroverov, R. Kobayashi, J. Normand, K. Raghavachari, A. Rendell, J. C. Burant, S. S. Iyengar, J. Tomasi, M. Cossi, N. Rega, J. M. Millam, M. Klene, J. E. Knox, J. B. Cross, V. Bakken, C. Adamo, J. Jaramillo, R. Gomperts, R. E. Stratmann, O. Yazyev, A. J. Austin, R. Cammi, C. Pomelli, J. W. Ochterski, R. L. Martin, K. Morokuma, V. G. Zakrzewski, G. A. Voth, P. Salvador, J. J. Dannenberg, S. Dapprich, A. D. Daniels, O. Farkas, J. B. Foresman, J. V. Ortiz, J. Cioslowski and D. J. Fox, *Gaussian 09, Revision A.01*, Gaussian, Inc., Wallingford, CT, 2009.
- 13 (a) P. J. Hay and W. R. Wadt, *J. Chem. Phys.*, 1985, **82**, 299; (b) M. M. Francel, W. J. Pietro, W. J. Hehre, J. S. Binkley, M. S. Gordon, D. J. Defrees and J. A. Pople, *J. Chem. Phys.*, 1982, **77**, 3654.
- 14 (a) A. F. Rausch, M. E. Thompson and H. Yersin, *Inorg. Chem.*, 2009, **48**, 1928.
- 15 (a) J. Kalinowski, W. Stampor, J. Mezyk, M. Cocchi, D. Virgili, V. Fattori and P. Di Marco, *Phys. Rev. B: Condens. Matter Mater. Phys.*, 2002, **66**, 235321; (b) W. S. Jeon, T. J. Park, S. Y. Kim, R. Pode, J. Jang and J. H. Kwon, *Appl. Phys. Lett.*, 2008, **93**, 063303.
- 16 S. C. Tse, H. H. Fong and S. K. So, *J. Appl. Phys.*, 2003, **94**, 2033.
- 17 (a) H. Scher and E. W. Montroll, *Phys. Rev. B: Solid State*, 1975, **12**, 2455; (b) A. J. Pal, R. Osterbacka, K. M. Kallman and H. Stubb, *Appl. Phys. Lett.*, 1997, **71**, 228.